EPJ Web of Conferences **191**, 05011 (2018) https://doi.org/10.1051/epjconf/201819105011
QUARKS-2018

Holographic study of Wilson loop in the anisotropic background with confinement/deconfinement phase transition

Pavel Slepov[1]*

[1]Moscow State University, Faculty of Physics, 1-2 Leninskie Gory, 119991, Moscow, Russia

Abstract. Within the bottom-up holographic QCD using anisotropic black brane solutions in 5D Einstein-dilaton-two-Maxwell system constructed in [1, 2], we study the temporal Wilson loops with arbitrary orientation in respect to the anisotropy direction. We calculate the minimal surfaces of the corresponding probing open string world-sheet in anisotropic backgrounds with various temperatures and chemical potentials. The dynamical wall locations, providing the quark confinement, depend on the orientation of the quark pairs, that gives a crossover transition line between confinement/deconfinement phases in the dual gauge theory.

1 Introduction

Study of the QCD phase diagram, as a function of temperature T and chemical potential μ, is one of the most important problems. The AdS/CFT duality provides an alternative tool for dynamics understanding of quark-gluon plasma (QGP) produced in the heavy-ions-collisions (HIC) [3–6].

It is believed that there are indications that QGP is anisotropic right after the collision of ions. Isotropisation occures at times $\sim$ 2 fm/s. It is natural to consider an anisotropic metric within the holographic approach. Anisotropy is usually provided by adding magnetic ansatz of Maxwell field to dilaton gravity action. Non-zero chemical potential is introduced via electic ansatz for the second Maxwell field. Thereby the 5-dimensional dilaton gravity with two Maxwell fields turns out to be the most suitable model. Such model was considered in [1, 7]. In the simplest case anisotropic Lifshitz-like models, characterized by anisotropic parameter ν, have been investigated [8].

We consider a 5-dimensional Einstein-dilaton-two-Maxwell system. In the Einstein frame the action of the system is specified as

$$S = \int \frac{d^5x}{16\pi G_5} \sqrt{-\det(g_{\mu\nu})} \left[R - \frac{f_1(\phi)}{4} F_{(1)}^2 - \frac{f_2(\phi)}{4} F_{(2)}^2 - \frac{1}{2} \partial_\mu \phi \partial^\mu \phi - V(\phi) \right], \qquad (1)$$

where $F_{(1)}^2$ and $F_{(2)}^2$ are the squares of the Maxwell fields $F_{\mu\nu}^{(1)} = \partial_\mu A_\nu - \partial_\nu A_\mu$ and $F_{\mu\nu}^{(2)} = q\, dy^1 \wedge dy^2$, $f_1(\phi)$ and $f_2(\phi)$ are the gauge kinetic functions associated with the corresponding Maxwell fields, $V(\phi)$ is the potential of the scalar field ϕ.

*e-mail: slepov@mi.ras.ru

To find the black brane solution in the anisotropic background, we used the metric ansatz in the following form:

$$ds^2 = G_{\mu\nu}dx^\mu dx^\nu = \frac{L^2\, b(z)}{z^2}\left[-g(z)dt^2 + dx^2 + z^{2-\frac{2}{\nu}}\left(dy_1^2 + dy_2^2\right) + \frac{dz^2}{g(z)}\right], \tag{2}$$

$$\phi = \phi(z), \qquad A_\mu^{(1)} = A_t(z)\delta_\mu^0, \tag{3}$$

$$F_{\mu\nu}^{(2)} = q\, dy^1 \wedge dy^2, \tag{4}$$

where $b(z)$ is the warp factor and $g(z)$ is the blackening function; we set the AdS radius $L = 1$. All the quantities in formulas and figures are presented in dimensionless units.

Note that in [1, 2] the following strategy to study holographic model is used. Firstly, one takes b suitable for phenomenological application, in particular one can take $b = e^{\frac{cz^2}{2}}$. Secondly, the anisotropic multiplier $z^{2-2/\nu}$ is also fixed by phenomenological reasons [8]. Thirdly, one takes a specific function f_1 by reasons of simplicity. And finally, using E.O.M. following from (2), one finds coupling function f_2, potential V, Maxwell field potential A_μ and blackening function g. The last one has the form:

$$g = 1 - \frac{z^{2+\frac{2}{\nu}}}{z_h^{2+\frac{2}{\nu}}}\,\frac{\mathfrak{G}(\frac{3}{4}cz^2)}{\mathfrak{G}(\frac{3}{4}cz_h^2)} - \frac{\mu^2 cz^{2+\frac{2}{\nu}}e^{\frac{cz^2}{2}}}{4\left(1-e^{\frac{cz_h^2}{4}}\right)^2}\,\mathfrak{G}(cz^2) + \frac{\mu^2 cz^{2+\frac{2}{\nu}}e^{\frac{cz^2}{2}}}{4\left(1-e^{\frac{cz_h^2}{4}}\right)^2}\,\frac{\mathfrak{G}(\frac{3}{4}cz^2)}{\mathfrak{G}(\frac{3}{4}cz_h^2)}\,\mathfrak{G}(cz_h^2), \tag{5}$$

where the function $\mathfrak{G}(x)$ has the following expansion:

$$\mathfrak{G}(x) = \sum_{n=0}^{\infty}\frac{(-1)^n x^n}{n!(1+n+\frac{1}{\nu})}. \tag{6}$$

2 The Wilson loop

The purpose of our consideration is to calculate the expectation value of the temporal Wilson loop

$$W[C_\vartheta] = e^{-S_{\vartheta,t}}, \tag{7}$$

oriented along vector $\vec{n}$, such that

$$n_x = \cos\vartheta, \quad n_y = \sin\vartheta. \tag{8}$$

Following the holographic approach [9–11] we have to calculate the value of the Nambu-Goto action for test string in our background:

$$S = -\frac{1}{2\pi\alpha'}\int d\xi^0 d\xi^1\,\sqrt{-\det h_{\alpha\beta}}, \tag{9}$$

where

$$h_{\alpha\beta} = G_{\mu\nu}\partial_\alpha X^\mu \partial_\beta X^\nu \tag{10}$$

and $G_{\mu\nu}$ is given by (2). The world sheet presented in Fig.1 is parameterized as

$$X^0 \equiv t = \xi^0,\ X^1 \equiv x = \xi^1\cos\vartheta,\ X^2 \equiv y_1 = \xi^1\sin\vartheta,\ X^3 \equiv y_2 = const,\ X^4 \equiv z = z(\xi^1). \tag{11}$$

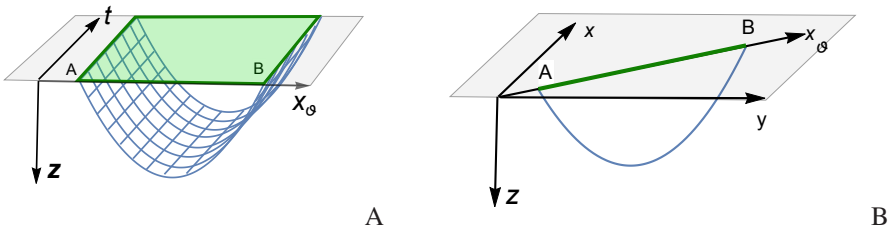

A B

Figure 1. A) Wilson loop and the world sheet. B) Projection of the world sheet to fixed t

We can use the following notation $\xi \equiv \xi^1$. In our case the action can be rewritten:

$$S = -\frac{\tau}{2\pi\alpha'}\int d\xi\, M(z(\xi))\sqrt{\mathcal{F}(z(\xi)) + (z'(\xi))^2}, \tag{12}$$

where $\tau = \int d\xi^0$,

$$M(z(\xi)) = \frac{b(z(\xi))}{z(\xi)^2}, \tag{13}$$

$$\mathcal{F}(z(\xi)) = g(z(\xi))\left(z(\xi)^{2-\frac{2}{\nu}}\sin^2(\theta) + \cos^2(\theta)\right). \tag{14}$$

The right-hand side of (12) defines the action of 1-dim dynamical model. This system possesses the first integral of motion:

$$I = \frac{M(z)\mathcal{F}(z)}{\sqrt{\mathcal{F}(z) + z'^2}}. \tag{15}$$

If we introduce z_{min} at which $z'(\xi) = 0$, then the first integral can be expressed as:

$$M(z_{min})\sqrt{\mathcal{F}(z_{min})} = I, \tag{16}$$

Let us introduce the effective potential:

$$\mathcal{V}(z(\xi)) \equiv M(z(\xi))\sqrt{\mathcal{F}(z(\xi))}. \tag{17}$$

In order to calculate the length of the curve, at first we have to find the character length of string:

$$\ell = \int_0^{z_{min}} \frac{2}{\sqrt{\mathcal{F}(z)}} \frac{dz}{\sqrt{\left(\frac{\mathcal{V}(z)}{\mathcal{V}(z_{min})}\right)^2 - 1}}, \tag{18}$$

where $\mathcal{V}(z) \equiv M(z)\sqrt{\mathcal{F}(z)}$.

3 Confinement/deconfinement phase transition

To find the conditions of the phase transition [7] we make an expansion of $\mathcal{V}^2(z)/\mathcal{V}^2(z_{min})$ in the Taylor series at the point z_{min}:

$$\frac{\mathcal{V}^2(z)}{\mathcal{V}^2(z_{min})} = 1 + \mathcal{V}_1 \cdot (z - z_{min}) + \mathcal{V}_2 \cdot (z - z_{min})^2 + o((z - z_{min})^2), \tag{19}$$

where

$$\mathcal{V}_1 \equiv \frac{2\mathcal{V}'(z_{min})}{\mathcal{V}(z_{min})}, \tag{20}$$

$$\mathcal{V}_2 \equiv \frac{\mathcal{V}(z_{min})\mathcal{V}''(z_{min}) + \mathcal{V}'(z_{min})^2}{\mathcal{V}^2(z_{min})}. \tag{21}$$

Therefore

$$\ell = 2\int_0^{z_{min}} \frac{dz}{\sqrt{\mathcal{F}(z)(\mathcal{V}_1 \cdot (z - z_{min}) + \mathcal{V}_2 \cdot (z - z_{min})^2)}}. \tag{22}$$

For the confinement/deconfinement phase transition the character length ℓ must be infinite for $z \to z_{min}$. So we have two different cases: $\mathcal{V}'(z) = 0$ and $\mathcal{V}'(z) \neq 0$.

1) If $\mathcal{V}'(z) \neq 0$ we can consider the first order only:

$$\ell = 2\int_0^{z_{min}} \frac{dz}{\sqrt{\mathcal{F}(z)\mathcal{V}_1(z - z_{min})}} \sim \sqrt{\frac{z - z_{min}}{\mathcal{F}(z_{min})\mathcal{V}_1}}, \tag{23}$$

so that $\ell \to 0$ as $z \to z_{min} - 0$.

2) If $\mathcal{V}'(z) = 0$ we have to use the second order:

$$\ell = 2\int_0^{z_{min}} \frac{dz}{\sqrt{\mathcal{F}(z)\,\mathcal{V}_2} \cdot (z_{min} - z)} \sim \frac{\log(z_{min} - z)}{\sqrt{\mathcal{F}(z_{min})\,\dfrac{\mathcal{V}''(z_{min})}{\mathcal{V}(z_{min})}}}, \tag{24}$$

so that $\ell \to \infty$ as $z \to z_{min} - 0$. Note that z_{min} really is the minimum of function $\mathcal{V}(z)$ as $\mathcal{V}'(z_{min}) \equiv 0$ and

$$\mathcal{V}(z) = \frac{M(z)\mathcal{F}(z)}{\sqrt{\mathcal{F}(z)}} > \frac{M(z)\mathcal{F}(z)}{\sqrt{\mathcal{F}(z) + z'^2}} = \frac{M(z_{min})\mathcal{F}(z_{min})}{\sqrt{\mathcal{F}(z_{min})}} = \mathcal{V}(z_{min}), \tag{25}$$

thus $\mathcal{V}''(z_{min}) > 0$. So to find stationary points of $\mathcal{V}(z)$ we should solve the following equation:

$$\mathcal{V}'(z) = 0. \tag{26}$$

The potential with the field of dilaton is:

$$\mathcal{V}_\theta(z) = \frac{b(z)e^{\sqrt{\frac{2}{3}}\phi(z)}}{z^2}\sqrt{g(z)\left(z^{2-\frac{2}{\nu}}\sin^2(\theta) + \cos^2(\theta)\right)}. \tag{27}$$

In our case the effective potential depends on the warp factor, the scalar field and the angle. To find stationary points of $\mathcal{V}(z)$ we solve the equation (26) for the potential (27) with arbitrary angle:

$$\begin{aligned}\mathcal{DW}_\theta \equiv cz \quad &+ \quad \frac{1}{\nu z}\sqrt{\frac{2}{3}}\sqrt{3c\,\nu^2 z^2\left(\frac{cz^2}{2} - 3\right) + 4\nu - 4} - \\ &- \quad \frac{2}{z} + \frac{\left(1 - \dfrac{1}{\nu}\right)z^{1-\frac{2}{\nu}}\sin^2(\theta)}{\cos^2(\theta) + z^{2-\frac{2}{\nu}}\sin^2(\theta)} + \frac{g'}{2g}\bigg|_{z=z_{DW\theta}} = 0.\end{aligned} \tag{28}$$

It is possible to obtain particular cases for $\theta = 0^0,\ 90^0$ [1, 2] from the expression (28):

$$\mathcal{DW}_x \equiv cz + \frac{1}{\nu z}\sqrt{\frac{2}{3}}\sqrt{3c\,\nu^2 z^2\left(\frac{cz^2}{2}-3\right)+4\nu-4}+\frac{g'}{2g}-\frac{2}{z}\Bigg|_{z=z_{DWx}}=0, \tag{29}$$

$$\mathcal{DW}_y \equiv cz + \frac{1}{\nu z}\sqrt{\frac{2}{3}}\sqrt{3c\,\nu^2 z^2\left(\frac{cz^2}{2}-3\right)+4\nu-4}+\frac{g'}{2g}-\frac{\nu+1}{\nu z}\Bigg|_{z=z_{DWy}}=0. \tag{30}$$

The expression for the temperature $T(z_h, \mu, c, \nu)$ is

$$T(z_h,\mu,c,\nu)=\frac{g'(z_h)}{4\pi}=\frac{e^{-\frac{3cz_h^2}{4}}}{2\pi z_h}\left|\frac{1}{\mathfrak{G}(\frac{3}{4}cz_h^2)}+\frac{\mu^2 c z_h^{2+\frac{2}{\nu}}e^{\frac{cz_h^2}{4}}}{4\left(1-e^{\frac{cz_h^2}{4}}\right)^2}\left(1-e^{\frac{cz_h^2}{4}}\frac{\mathfrak{G}(cz_h^2)}{\mathfrak{G}(\frac{3}{4}cz_h^2)}\right)\right|. \tag{31}$$

Let us remind that in [1, 2] the thermodynamical properties of the constructed black hole background were studied and the large/small black hole phase transitions (BB-transition) were found at the temperature $T_{BB}(\mu)$. Hawking-Page phase transition takes place at $z_{h,HP}$, where the free energy equals zero. The particular value of $z_{h,HP}$ depends on c and ν and is larger for larger negative c, i.e. $z_{h,HP}(c_1,\nu) < z_{h,HP}(c_2,\nu)$ for $c_1 < c_2 < 0$. For the anisotropic background the Hawking-Page horizon is less than for the isotropic one with the same $c < 0$.

At $\mu = 0$ and for $T < T_{HP}(0)$ the black hole dissolves to thermodynamically stable thermal gas. If the system cools down with the non-zero chemical potential less than some critical value μ_{cr}, the background undergoes the phase transition from a large to a small black hole. This is a generalization of the corresponding effect in the isotropic case [12–16]. The temperature of the large/small black hole phase transition in anisotropic case is less than in the isotropic one, i.e. $T_{BB}^{(aniso)}(\mu) < T_{BB}^{(iso)}(\mu)$. The value of the critical chemical potential, up to which this phase transition exists, is bigger in the anisotropic case compared to the isotropic one, $\mu_{cr}^{(\nu)} > \mu_{cr}^{(iso)}$. Also, the point $(\mu_{cr}^{(\nu)}, T_{cr}^{(\nu)})$ for $\nu \to 1$ goes smoothly to $(\mu_{cr}^{(iso)}, T_{cr}^{(iso)})$.

In Fig.2–4 we can see the angle dependence of the confinement/deconfinment phase transition on the Wilson loop orientation. We choose $\theta = 0^0,\ 10^0,\ 45^0,\ 60^0,\ 90^0$. In the boundary cases the graphs coincide with the graphs for W_x (blue solid line) and W_y (magenta solid line) from [1, 2].

In our consideration we take into account the Hawking-Page phase transition (dashed pink line). For the critical angle $\theta_{cr1} = 22^0$ (green dashed line) the Wilson loop phase transition line intersects the Hawking-Page phase transition line at it's very end point from above. For the critical angle $\theta_{cr2} = 54^0$ (dashed cyan line) the top point $\mu = 0$ of the confinement/deconfinement phase transition for the Hawking-Page line and the Wilson loop line is chosen to be the same. In Fig.3 we see, that in this case the Hawking-Page phase transition line coincides with the Wilson loop line along the entire length. From this angle the Wilson loop line fully determines confinement/deconfinement phase transition. This situation preserves up to the next critical angle $\theta_{cr3} = 78^0$ (light pink dashed line). Here the Wilson loop phase transition line intersects the Hawking-Page phase transition line at it's very end point from below.

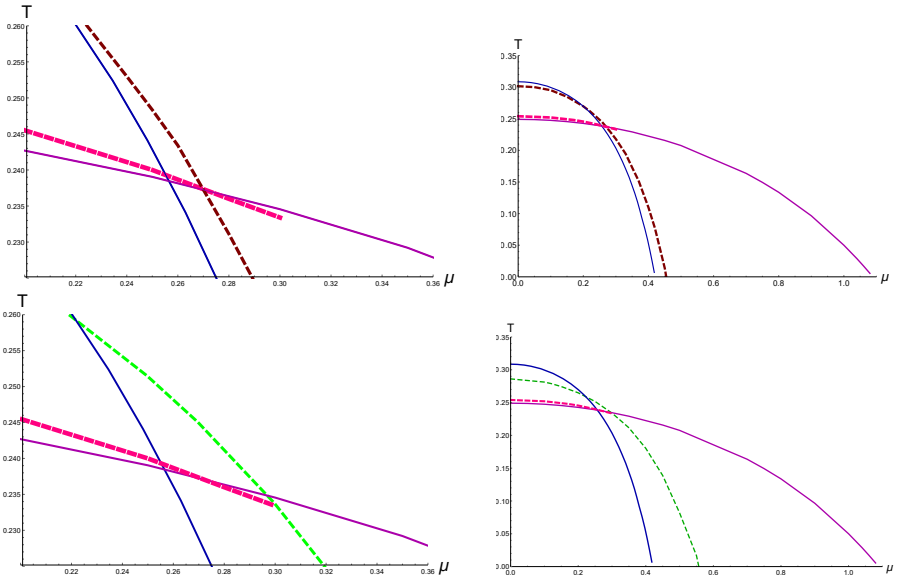

Figure 2. Phase transition diagrams for $\theta = 10^0$ (brown dashed line, upper pictures) and $\theta_{cr1} = 22^0$ (green dashed line, lower pictures) in details in selected region on the left side and in general on the right side.

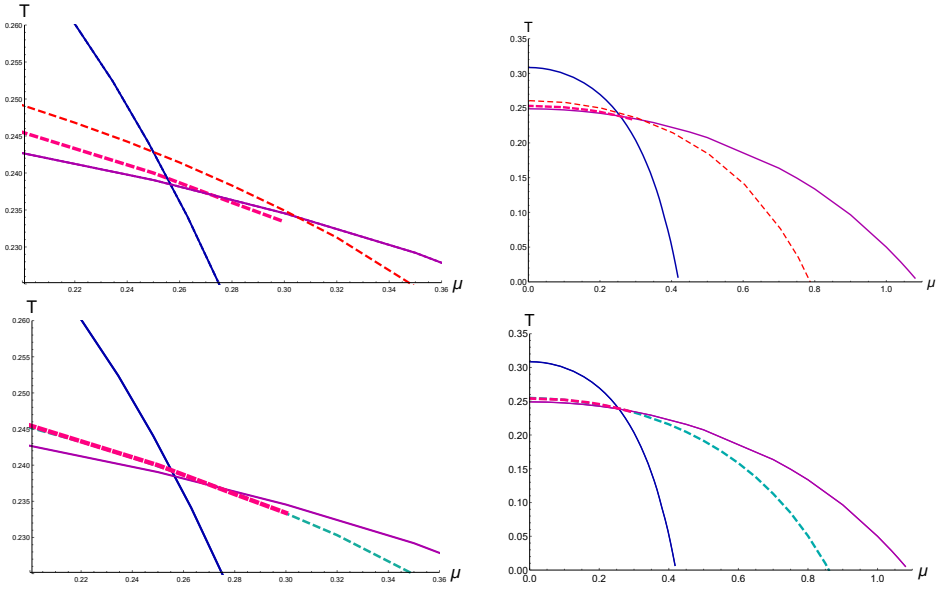

Figure 3. Phase transition diagrams for $\theta = 45^0$ (red dashed line, upper pictures) and $\theta_{cr2} = 54^0$ (cyan dashed line, lower pictures) in details in selected region on the left side and in general on the right side.

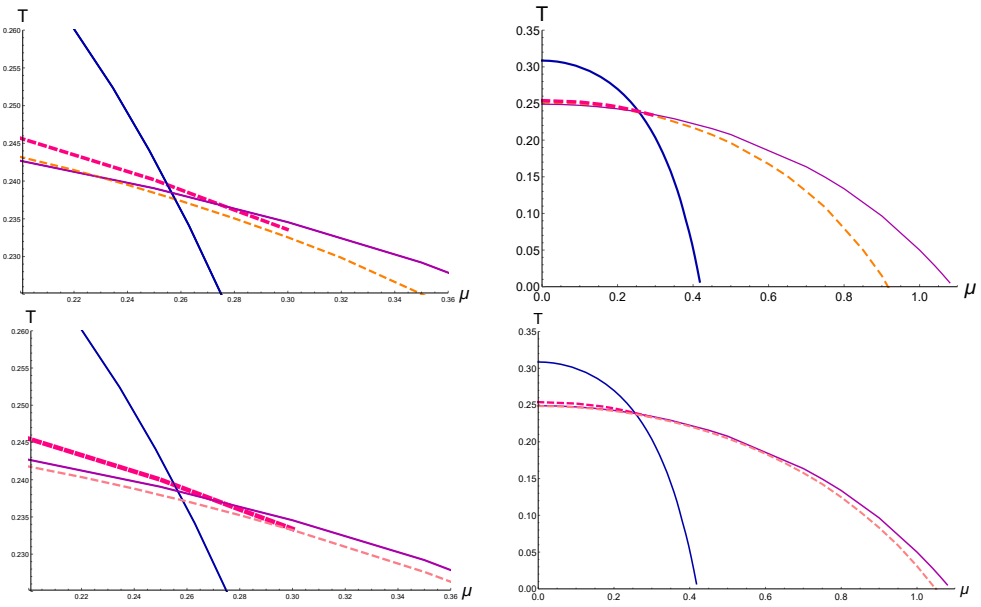

Figure 4. Phase transition diagrams for $\theta = 60^0$ (orange dashed line, upper pictures) and $\theta_{cr3} = 78^0$ (light pink dashed line, lower pictures) in details in selected region on the left side and in general on the right side.

4 Conclusion

We have studied the dependence of behavior of the temporal Wilson loops on the orientation specified by arbitrary angle θ in the background (2). This result is the generalization of the two particular cases of orientation, considered in [1, 2], that can be associated with boundary values $\theta = 0^0, 90^0$.

We demonstrated that the phase diagram depends on the orientation [7]. Taking into account the instability zones of the anisotropic background, we have found more complicated confinement/deconfinement phase diagrams for differently oriented temporal Wilson loops. For this purpose we have studied the behavior of the temporal Wilson loops in the particular 5-dimensional anisotropic background supported by dilaton and two-Maxwell field. The diagram is defined in (μ, T)-plane for arbitrary angles.

In this model we have determined the critical angles $\theta_{cr1} = 22^0$, $\theta_{cr2} = 54^0$, $\theta_{cr3} = 78^0$. For the critical angle $\theta_{cr1} = 22^0$ the part of confinement/deconfinement phase transition line is determined by the Hawking-Page phase transition. For the angle $\theta_{cr2} = 54^0$ the top point of the Hawking-Page phase transition coincides with the top point of the confinement/deconfinement phase transition. For the $\theta_{cr3} = 78^0$ the whole confinement/deconfinement phase transition line is determined by the Wilson loop.

More detailed consideration for the arbitrary orientation is presented in [17]. In all likelihood these calculations are relevant in the context of the future NICA and FAIR projects.

Acknowledgments

This paper is based on a talk at the XXth International Seminar on High Energy Physics "Quarks-2018" at Valday, Russia on 27 May - 2 June 2018. Author would like to thank the

organizers of Quarks-2018 for the support. Author would like to thank Irina Arefeva and Kristina Rannu for useful discussions.

References

[1] I. Aref'eva and K. Rannu, JHEP **05**, 206 (2018)
[2] K. Rannu, talk "Holographic anisotropic background with confinement-deconfinement phase transition" on the XXth International Seminar "Quarks-2018".
[3] J. Casalderrey-Solana, H. Liu, D. Mateos, K. Rajagopal, U. Wiedemann, Cambridge University Press, (2014)
[4] I. Aref'eva, Phys. Usp. **57**, 527 (2014)
[5] I. Aref'eva, talk "Holography for Heavy Ions Collisions at LHC and NICA" on the XXth International Seminar "Quarks-2018".
[6] O. DeWolfe, S. Gubser, C. Rosen and D. Teaney, Prog. Part. Nucl. Phys. **75**, 86 (2014)
[7] I. Aref'eva, EPJ Web Conf. **164**, 01014 (2017)
[8] I. Aref'eva, A. Golubtsova and E. Gourgoulhon, JHEP **1609**, 142 (2016)
[9] J. Maldacena, Phys. Rev. Lett. **80**, 4859 (1998)
[10] S. Rey, S. Theisen and J. Yee, Nucl. Phys. **B 527**, 171 (1998)
[11] A. Brandhuber, N. Itzhaki, J. Sonnenschein and S. Yankielowicz, Phys. Lett. **B 434**, 36 (1998)
[12] A. Chamblin, R. Emparan, C. Johnson and R. Myers, Phys. Rev. D **60**, 064018 (1999)
[13] O. DeWolfe, S. Gubser and C. Rosen, Phys. Rev. D **83**, 086005 (2011)
[14] O. DeWolfe, S. Gubser and C. Rosen, Phys. Rev. D **84**, 126014 (2011)
[15] S. He, S.-Y. Wu, Y. Yang and P.-H. Yuan, JHEP **04**, 093 (2013)
[16] Y. Yang and P.-H. Yuan, JHEP **1512**, 161 (2015)
[17] I. Aref'eva, K. Rannu and P. Slepov, arXiv:1808.05596 [hep-th] (2018)